International Conference on Space Optics—ICSO 2018

Chania, Greece

9–12 October 2018

Edited by Zoran Sodnik, Nikos Karafolas, and Bruno Cugny

The CubeSat Laser Infrared CrosslinK Mission (CLICK)

Kerri Cahoy

Peter Grenfell

Angela Crews

Michael Long

et al.

esa icso proceedings cnes

International Conference on Space Optics — ICSO 2018, edited by Zoran Sodnik, Nikos Karafolas, Bruno Cugny, Proc. of SPIE Vol. 11180, 111800Y · © 2018 ESA and CNES · CCC code: 0277-786X/18/$18 · doi: 10.1117/12.2535953

The CubeSat Laser Infrared CrosslinK Mission (CLICK)

Kerri Cahoy*[a], Peter Grenfell[a], Angela Crews[a], Michael Long[a], Paul Serra[a], Anh Nguyen[c], Riley Fitzgerald[a], Christian Haughwout[a], Rodrigo Diez[a], Alexa Aguilar[a], John Conklin[b], Cadence Payne[a], Joseph Kusters,[a] Chloe Sackier[a], Mia LaRocca[a], Laura Yenchesky[a]
[a]Massachusetts Institute of Technology, Department of Aeronautics and Astronautics, 77 Mass. Ave., Cambridge, MA, USA 02139; [b]University of Florida, Department of Mechanical & Aerospace Engineering, 231 MAE-A, P. O. Box 116250, Gainesville, FL, USA 32611; [c]NASA Ames Research Center, Moffett Blvd., Mountain View, CA, USA 94035

ABSTRACT

The CubeSat Laser Infrared CrosslinK mission is a joint Massachusetts Institute of Technology (MIT), University of Florida (UF), and NASA Ames Research Center effort to develop laser communications (lasercom) transceivers. The terminals demonstrate full-duplex intersatellite communications and ranging capability using commercial components to enable future large constellations or swarms of nanosatellites as coordinated distributed sensor systems.

CLICK will demonstrate a crosslink between two CubeSats that each host a < 2U lasercom payload. Range control is achieved using differential drag in Low Earth Orbit (LEO), with attitude controlled using a three-axis reaction wheel assembly and attitude sensors, including star trackers.

The lasercom terminals are direct-detect and rate scalable, designed to achieve a 20 Mbps crosslink at ranges from 25 km to 580 km and operate full-duplex at 1537 nm and 1563 nm with 200 mW of transmit power and a 14.6 arcscecond (0.07 milliradian) full width half max (FWHM) beamwidth. The terminals also use a 976 nm, 500 mW, 0.75 degree FWHM beacon and a quadcell for initial acquisition, and a low-rate radio crosslink for exchanging orbit information.

The payload transmitter is a master oscillator power amplifier (MOPA) with fiber Bragg grating for pulse shaping and MEMS fast steering mirror (FSM) for fine pointing, modeled after the MIT Nanosatellite Optical Downlink Experiment. The transceiver leverages UF's Miniature Optical Communications Transmitter (MOCT) including a chip-scale atomic clock (CSAC). The receiver implements both a time to digital converter (TDC) as well as pulse recovery and matched filtering for precision ranging.

Keywords: crosslink, intersatellite, free space optical, laser, CubeSat, pulse position modulation

1. INTRODUCTION

Small satellite missions have the potential to improve spatial and temporal coverage of the Earth, with the lower cost of commercial components and ride-share access to space enabling constellations of larger numbers of satellites or formation-flying swarms. Miniaturized instruments for small satellites are becoming increasingly data intensive, for example, hyperspectral imagers, videography, and wideband software defined radios. Coordinated distributed aperture applications can require shared precision ranging and timing information. Defense applications also require link security and robustness to failure of network nodes. The challenge is to provide high-rate connectivity between spacecraft and to the ground, with precision range and time transfer, using a transceiver architecture that is compact, power efficient, handles dynamic range and velocity conditions, and leverages commercially available components to be consistent with high volume manufacturing for nanosatellite platforms. Due to the much smaller wavelength and beam size of infrared light relative to radio frequencies, laser communications (lasercom) implementations can be more size, weight, and power (SWaP) efficient. The narrower beam makes the signal more difficult to intercept, and currently optical wavelengths have access to bandwidth with few regulatory and licensing constraints.

The Cubesat Infrared CrosslinK (CLICK) mission is a collaboration between the Massachusetts Institute of Technology (MIT) Space, Telecommunications, Astronomy, and Radiation Laboratory (STAR Lab), the Precision Space Systems Laboratory at the University of Florida (UF), and NASA Ames Research Center to develop a pair of CubeSats to demonstrate a nanosatellite crosslink as well as a downlink to a MIT portable optical ground station [1]. The two lasercom payload terminals are designed to achieve crosslink communications rates of at least 20 Mbps at ranges from 25 km to 580 km or more, with ranging capability better than 50 cm (1.6 ns timing).

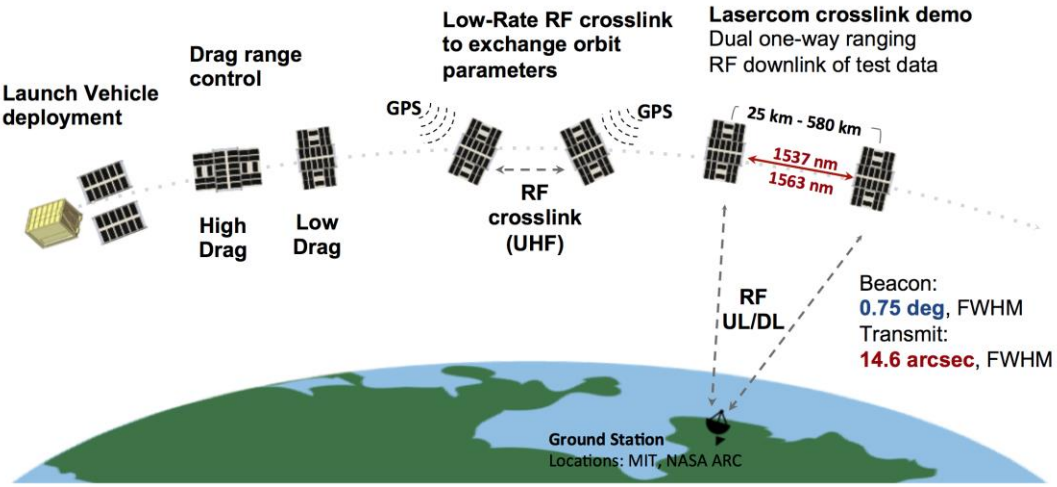

Figure 1. CLICK mission Concept of Operations. Two CubeSats are deployed in low Earth orbit (LEO) at an altitude of approximately 500 km. The satellites do not require propulsion but rather drag management, where the reaction-wheel based CubeSat attitude determination and control system (ADCS) maintains high drag (larger surface area in the direction of travel) or low drag orientations as needed to adjust intersatellite range. For the initial demonstration, the CubeSats can exchange orbit and attitude information via a low-rate radio frequency crosslink, which could be a UHF radio or even leverage something like a Globalstar duplex modem. Each CubeSat also has a GPS receiver for the initial demonstration, for orbit determination and time reference. Once the CubeSats are at the desired range, a wider 0.75 degree FWHM beacon at 976 nm is used for coarse acquisition, before transitioning to the narrower 14.6 arcsecond FWHM full-duplex crosslink. Low-rate radio links to ground stations are used for command and control, which could also be done with a Globalstar duplex modem.

Table 1. Comparison of full width half max (FWHM) beam divergences and link parameters for a few example lasercom missions. The Aerocube Optical Communication and Sensor Demonstration [2,3] and the MIT Nanosatellite Optical Downlink Experiment [4] are CubeSat platforms; the Optical Space Infrared Downlink System (OSIRIS) Bi-spectral InfraRed Optical System (BIROS) [5], the Lunar Laser Communications Demonstration (LLCD) [6,7], and the Near Field Infrared Experiment (NFIRE) [8] are on small satellite or larger platforms.

Mission	Beam Divergence Angle	Link Type
Aerocube7 OCSD A	540 arcsec (2.62 mrad)	LEO to Ground
Aerocube7 OCSD B	180 arcsec (872 urad)	LEO to Ground
CLICK A	268 arcsec (1.3 mrad)	LEO to Ground
BiROS OSIRIS	41.2 arcsec (200 urad)	LEO to Ground
NFIRE	14.8 arcsec (71.8 urad)	LEO to LEO
CLICK B&C	**14.6 arcsec (70.8 urad)**	**LEO to LEO or Ground**
LLCD	0.515 arcsec (2.5 urad)	Lunar to Ground

One of the major challenges in lasercom is the development of a pointing, acquisition, and tracking (PAT) system to establish and maintain the laser links. Table 1 lists the beamwidths for a few example nanosatellite, small satellite, or larger lasercom terminals. Due to the narrow transmission beam (e.g., 14.6 arcseconds for the CLICK terminal), PAT typically consists of a coarse pointing system with a wide field of view and limited precision supplemented by a fine pointing system with a narrow field of view but high precision. The CLICK coarse pointing system directly utilizes the spacecraft's attitude determination and control system (ADCS). The fine pointing system (FPS) uses a commercially available microelectromechanical system (MEMS) fast-steering mirror (FSM) controlled via feedback from a quadrant photodiode detector (quadcell), which also senses the beacon.

This paper will first briefly summarize the relevant CLICK mission requirements for the FPS control system design. A summary of previously generated performance estimates will then be given. The modeling approach will be described and the simulation results to date will be given. Finally, future work for improvements to the FPS control system will be outlined.

Table 2: Example intersatellite laser communications link budget for the CLICK mission.

Inter-satellite Crosslink Budget	
Range (km)	855.00
PPM Order	16.00
Transmit Power (dBW)	-6.99
Full Width Half Maximum (mrad)	0.07
Beam Solid Angle (steradians)	3.96E-09
Transmitter Gain (dBi)	95.02
Transmitter Loss (dB)	-1.74
Receiver Gain (dBi)	92.16
Receiver Loss (dB)	-1.75
Path Loss (dB)	-257.54
Atmospheric Loss (dB)	0.00
Pointing Loss (dB)	-3.00
Power Received (dBW)	-83.36
Power Required (dBW)	-86.44
Margin	**2.98**

1.1 Fine Pointing Requirement

The communications link budget (see Table 2) allots 3 dB loss due to pointing error, which corresponds to pointing within the full-width, half-max (FWHM) divergence angle of 14.6 arcsec (full-cone). Assuming symmetric pointing error, which is reasonable as discussed in Section 2, the resulting single-axis pointing requirement is ±5.18 arcsec. As discussed in Long [9], the contributions to this error include the residual pointing error from the FPS control system as well as error from optical, mechanical, and environmental sources. Contributors to the FPS control error include the sensor noise, spacecraft jitter, and the inertial coarse pointing error. Following the methodology in Long [9], the baseline FPS control error is estimated as ±2.27 arcsec. The mechanical and environmental errors include launch-induced shift, thermoelastic deformation, and residual misalignment following mechanical assembly and calibration. This error is estimated as ±4.50 arcsec [9]. The optical source of error, chromatic shift, is estimated as ±1.06 arcsec [9]. The total estimated error via RMS is ±5.15 arcsec, which results in a narrow margin of 0.6% to meet the 3 dB pointing loss requirement. The primary goal of this work is to improve this margin by further analysis and design refinement of the flight-level FPS control system. Improvements to mechanical, thermal, and chromatic shift error are not considered in this paper but are ongoing parallel efforts. The estimated FPS control error incorporates measurements from preliminary prototype experiments [10]. As a first prototype, the hardware used did not include flight-level electrical and optical

components or use the flight laser wavelength. The control law used was a digital integrator tuned using in-place calibration. This paper examines the FPS control error using a simulation created in MATLAB/Simulink®. This is used to rapidly test different control laws and tune parameters without risk to the actual hardware. It is also used to verify system requirements for the selected flight hardware before prototyping. Last, it allows analysis of the primary sources of error to better focus efforts for the refinement of the design. This paper presents the results of the first iteration of the simulation software, focusing on the development of the model and the control law development.

2. CLICK FINE POINTING SYSTEM

The payload optical system layout is shown in Fig. 2. As shown, there are three optical paths: the beacon Rx signal and the communications Tx and Rx signals. The objective of the fine pointing system (FPS) is to align the communications Tx and Rx signals to within the pointing requirement. The FPS is depicted in Fig. 3. The component selection and optical design of the system is detailed in Long [9]. The laser spot sensor is a First Sensor QP1-6 quadrant photodiode detector ("quadcell"), which consists of 4 Silicon PIN photodiode sensors evenly arranged in a rectangular pattern. The beacon signal (see Fig. 2) is detected on the quadcell, and the output signals are amplified and filtered via a transimpedance amplifier and a bandpass filter, respectively, as described in Long [9].

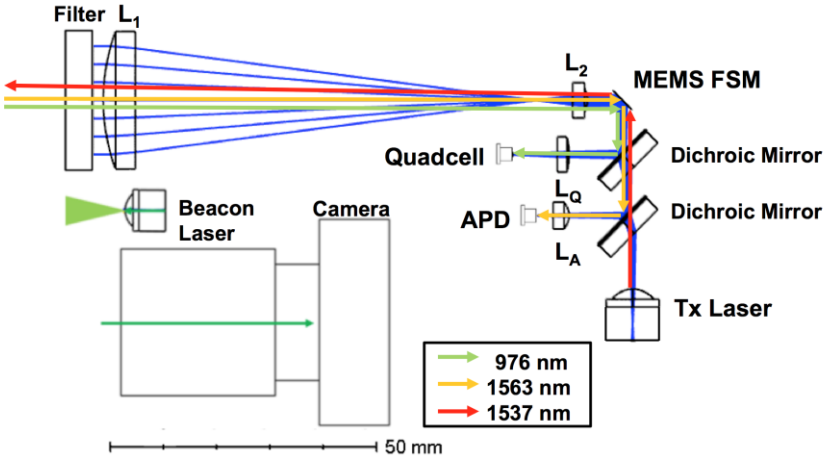

Figure 2. CLICK Payload Optical Layout.

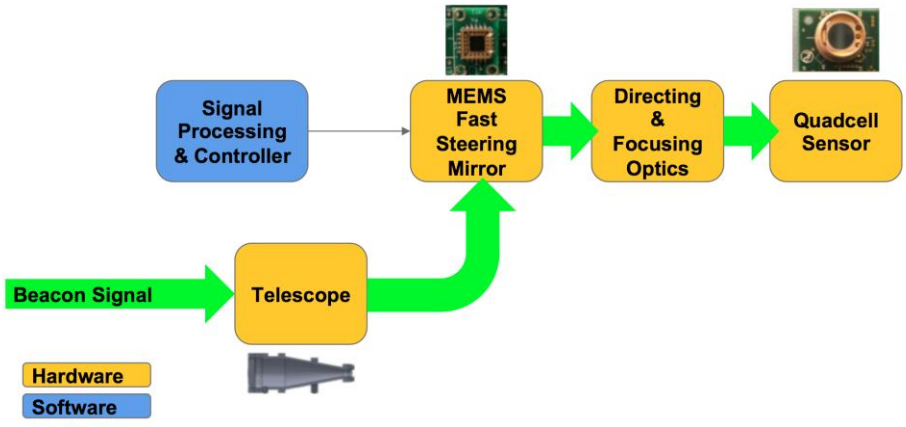

Figure 3. CLICK fine pointing system diagram.

The analog output signals are sampled by an Analog to Digital Converter (ADC) and routed to a Raspberry Pi Compute Module 3, which uses a Broadcom BCM2837 processor [11]. The X and Y centroids are calculated from the quadcell measurements and used by the controller. The resulting control signals are converted to analog signals, amplified, and then filtered via a 6th order Bessel low-pass filter before being routed to the Mirrorcle MEMS FSM. The FSM uses a Differential Quad-channel scheme to actuate a 3.6 mm diameter mirror, which has a maximum mechanical angle of ±3.2 degrees in both the X and Y axes [12,13].

The FPS was modeled in MATLAB/Simulink® with three primary model elements: the inertial pointing error, the optical system, the electronics, and reaction wheel jitter.

2.1 Review of the Coarse Pointing System

One of the more common PAT architectures consists of a large gimbal that the optical bench is mounted to [16,17,18]. In this type of design, the optical bench includes the fine pointing and tracking system, and the gimbal is used for coarse pointing, acquisition, and tracking. However, in order to meet the low-SWaP requirements of a CubeSat, the CLICK payload does not use a coarse pointing gimbal. Instead, it directly relies on the ADCS of the spacecraft, which is aided by a CMOS camera and wide angle (2700 arcseconds full-cone) beacon laser. This approach was initially developed by Yoon [10], and the modeling software has been maintained for continued design iteration. The inertial pointing error data used in this work was generated with Yoon's software.

2.2 Residual Inertial Pointing Error

The largest disturbance in the fine pointing system is due to the residual inertial pointing error from the attitude control system, which serves as the coarse pointing actuator for the PAT system. This error signal is generated from the coarse pointing model of the satellite, the details of which are described in Yoon [10].

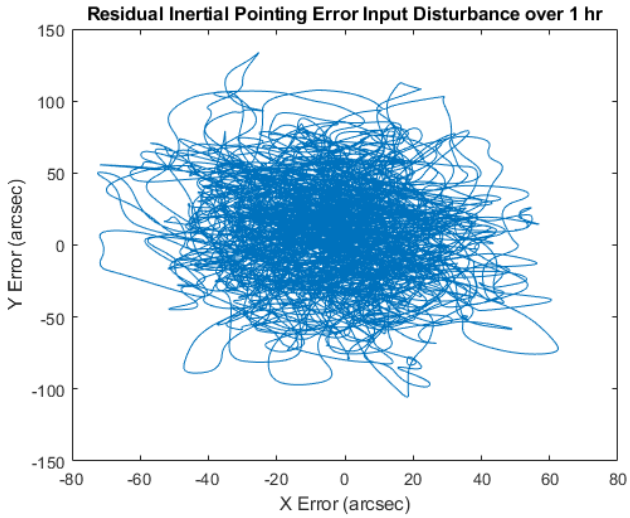

Figure 4: X-Y field angle from inertial pointing error.

The satellites are each equipped with a GPS unit and an RF crosslink for relaying GPS ephemerides between them. The payload contains a beacon system that utilizes a 10 degree FOV CMOS camera to measure the beacon signal (see Fig. 2). The coarse pointing system uses these two measurements of the relative state of the two satellites in order to estimate the relative pointing direction between them, which is the unit vector along the relative displacement vector. These measurements are synthesized in a specialized extended Kalman filter derived in Yoon [10]. The coarse pointing simulation also contains a model of the spacecraft dynamics including environmental disturbances as well as the attitude determination and control system. The environmental disturbances modeled so far include the gravity gradient torque and the magnetic dipole torque. Additional disturbances are currently modeled by Gaussian white noise. The results in this paper were derived from a coarse pointing simulation that was run for 1 hour of spacecraft time. The data was then transferred to the fine pointing system model, where a random time interval of 1 min, excluding the ADCS settling time, was selected and used as the residual inertial pointing error model. The field angle dynamics are shown in Figs. 4 and 5.

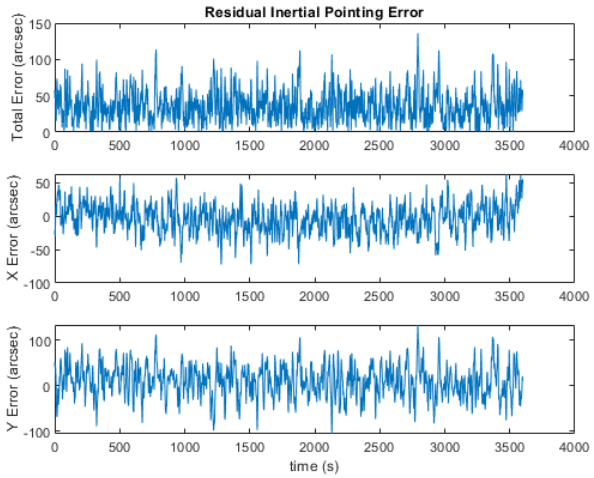

Figure 5: Timeseries of inertial pointing error.

The total pointing error is the RMS of the X and Y component errors and is therefore modeled effectively by a Rician distribution as shown in Fig. 6. The noncentrality parameter of this distribution is 2.55 with a 95% confidence interval of (0.00, 9.24). The X and Y distributions are approximately Gaussian. The X fit gives a mean pointing error of -4.00 arcsec within (-4.21, -3.78) with 95% confidence and a standard deviation of 20.94 arcsec within (20.79, 21.10) with 95% confidence. The Y fit gives a mean pointing error of 9.83 arcsec within (9.47, 10.19) with 95% confidence and a standard deviation of 34.74 arcsec within (34.74, 35.00) with 95% confidence.

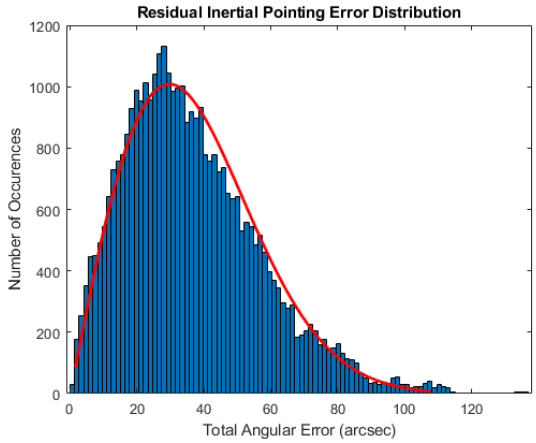

Figure 6: Rician distribution of inertial pointing error.

2.3 Optical Models

The optical modeling of the payload is complicated by the fact that the system operates at different wavelengths. As described in Long [9], the telescope design is optimized for the communications wavelengths of 1537 nm and 1563 nm, which means that the 976 nm beacon signal is not collimated at the exit pupil of the resizing telescope. In order to accurately model the beacon spot location on the quadcell as a function of the FSM tilt angle and the input field angle, a Zemax® model (see Fig. 7) is utilized. For this iteration of the model, decoupled X and Y axis dynamics were assumed, which is supported by Yoon [10] and the manufacturer [12,13]. The Y axis dynamics were used for this iteration of the model. The optical transfer functions to quadcell from the telescope aperture and from the FSM were estimated

independently for the range of angles, that covered the quadcell's 1.13 mm sensor diameter. The transfer functions models are affine for the small range of maximum angles of the input disturbance: 134 arcsec in Y and 72.5 arcsec in X. The affine transfer function from the field angle to the quadcell Y axis centroid is -1.057 um/arcsec with a bias of -0.021 um and an R2 value of 1. The affine transfer function from the FSM tilt angle to the quadcell Y axis centroid is 0.186 um/arcsec with a bias of 0.001 um and an R2 value of 1.

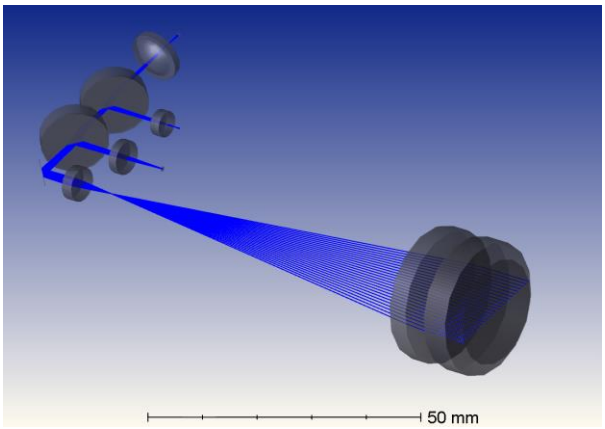

Figure 7: Zemax® Model of CLICK Payload Optics.

2.4 Electrical Models

Two simplifying assumptions were made about the electronics for this iteration of the system model. Future model iterations will include higher fidelity electronic models to anticipate sources of error due to digital sampling rates and software delays. The sampling rate on the ADC was assumed to be significantly larger than the inertial error dynamics, which is reasonable since the inertial pointing dynamics are estimated via power spectral density as being less than 3 Hz. Therefore, a continuous time version of the controller was used. The second simplification was to replace the quadcell sensor dynamics with an inverse system model that converts the quadcell position to a voltage in the range that is useable by the Raspberry Pi. The sensor dynamics, amplification, and filtering electronics will be included in future model iterations. The FSM is designed to minimize X-Y coupling [12,13], so the system is modeled at this stage by treating these as independent degrees of freedom. The open-loop FSM dynamics were modeled using a simple-harmonic-oscillator (SHO) for the FSM in series with the 6th order Bessel low-pass filter. The FSM transfer function is given in Eqn. 1.

$$G_{FSM}(s) = \frac{K\omega_n^2}{s^2+\frac{\omega_n}{Q}s+\omega_n^2} \tag{1}$$

Control design using the SHO model has been verified on the hardware by the manufacturer [12]. The parameters were taken from the specification sheet for part number S7105, which uses A1B1.4 actuators and a 3.6 mm diameter mirror. The DC gain K = 0.0252 deg/V. The natural frequency is 3.10 x 103 rad/s, and the quality factor Q = 20. Specifications for all Mirrorcle FSMs can be found at their website [14]. The 6th order Bessel low pass filter transfer function is shown in Eqn. 2.

$$G_{LPF}(s) = \frac{a_0}{s^6+a_5s^5+a_4s^4+a_3s^3+a_2s^2+a_1s+a_0} \tag{2}$$

The defining parameter is the 200 Hz cutoff frequency, and the purpose of the filter is to eliminate the resonance modes associated with the FSM, which can easily damage the MEMS assembly. The effect of the filter is shown in Fig. 8. The use of this filter has been verified on the hardware by the manufacturer [12] as well as in previous experiments [10,15]. The frequency responses of each of these transfer functions, as well as the overall open-loop system, are shown in Fig. 9. The gain margin is 17.70 dB, and the phase margin is infinite, which shows that the baseline open-loop pointing system

is stable and relatively robust to sources of error. The optics are designed to align the Rx and Tx beams when the beacon beam is centered on the quadcell. The closed-loop system design therefore focuses on rejecting disturbances like inertial pointing error and jitter.

2.5 Jitter Model

The last element of the forward path is reaction wheel jitter, which is modeled as a low-frequency noise signal generated by passing Gaussian white noise of intensity 0.10 arcsec through a 2nd order, 1 Hz cutoff low-pass filter. This is an approximation of the model of a BCT 15 to payload frequency response given in Shields et al. [19]. This simplification of the model does not include potential resonance effects. Further structural analyses and experiments are ongoing to develop a high-fidelity jitter model for the CLICK spacecraft.

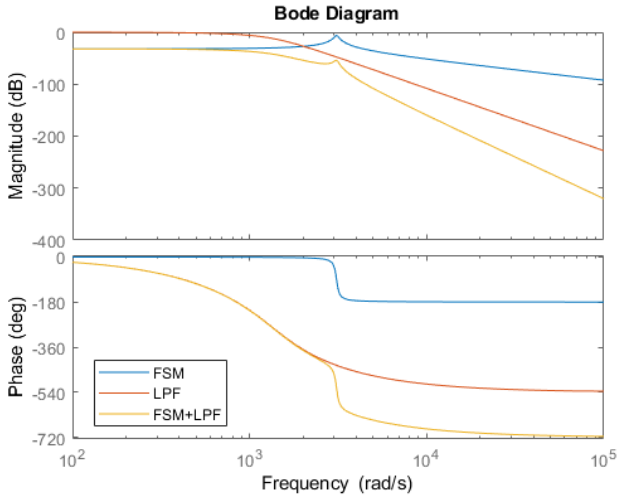

Figure 8. FSM & Low-Pass Filter (LPF) frequency responses

3. FPS CONTROL SYSTEM RESULTS

The controller chosen was a Proportional-Integral (PI) controller as shown in Eqn. 3. The derivative term of the typical PID is excluded to avoid noise amplification. The gains were tuned in place to values of KP = 1, KI = 100. The primary error correction is due to integration, which results in a more stable response compared to more heavily weighting the proportional control.

$$G_C(s) = K_P + \frac{K_I}{s} \tag{3}$$

The main results using the models described so far and these parameters are shown in Figs. 9 and 10. Fig. 9 shows the spot location of the beacon signal on the quadcell and where the uncontrolled disturbance signal would be. The average measured Y centroid error with the control is -0.0149 um with a standard deviation of 0.574 um. The corresponding pointing equivalent angle (PEA) is shown in Fig. 8. The average PEA is -0.0056 arcsec with a standard deviation of 0.543 arcsec, which corresponds to an error within the 3σ interval (-1.63, 1.62) arcsec. This is a 28% reduction in pointing error relative to the previous estimate of ±2.27 arcsec (3σ).

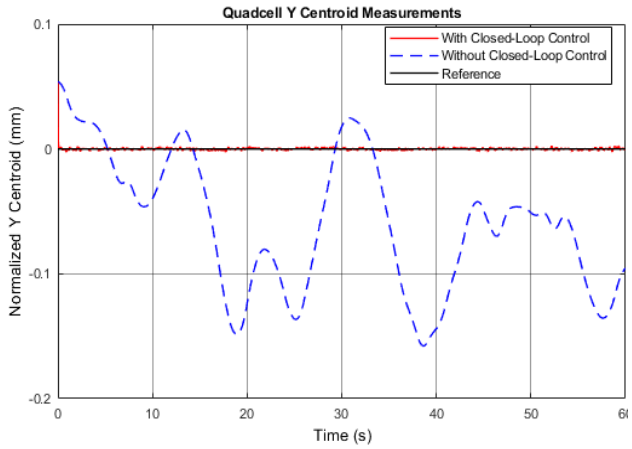

Figure 9. Quadcell Y-Axis Centroid Control Result

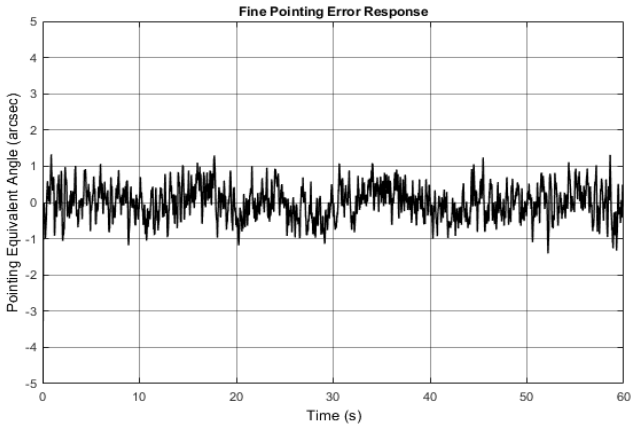

Figure 10. Fine Pointing Error.

4. CONCLUSION

The need for a high-fidelity simulation of the FPS control system was identified as a result of narrow design margins from design estimates to date. Models of the residual inertial pointing error, optical system, simplified electronics, and reaction wheel jitter were implemented in a closed-loop, PI control system. The initial results give an improvement in fine pointing error due to the FPS control error of 28%: from ±2.27 arcsec (3σ) to ±1.63 arcsec (3σ). This results in an overall improvement of fine pointing error of 4.8%: from ±5.15 arcsec (3σ) to ±4.90 arcsec (3σ) and an increase in margin from 0.06% to 5.4%. Improvements in the optomechanical sources of error will be part of future work. Future improvements to the simulation include i) body pointing aerodynamic and solar radiation pressure disturbance modeling, ii) higher fidelity modeling of the quadcell sensor electronics, iii) robustness to small cross-coupling in the FSM transfer function matrix, iv) assessment of failure modes like loss of GPS-lock, v) digital control modeling, vi) improved jitter modeling, and vii) assessment of alternative control techniques (e.g. H-Infinity).

REFERENCES

[1] Riesing, K.M., "Portable Optical Ground Stations for Satellite Communication," Ph.D. Thesis, Massachusetts Institute of Technology, 2018.

[2] Rowen, D. et al., "OCSD-A/Aerocube-7A status update." http://mstl.atl.calpoly.edu/ bklofas/Presentations/DevelopersWorkshop2016/, April 2016. Accessed: July 2018.

[3] Janson, S. et al., "The NASA Optical Communications and Sensor Demonstration Program: Mission Overview," AIAA / USU Small Satellite Conference, August 4-9, 2018, Logan Utah.

[4] Clements, E. et al., "Nanosatellite optical downlink experiment: design, simulation, and prototyping," Optical Engineering, 55(11), 111610 (2016). https://doi.org/10.1117/1.OE.55.11.111610.

[5] Schmidt, C. et al., "OSIRIS Payload for DLR's BiROS Satellite." In International Conference on Space Optical Systems and Applications, January 2014.

[6] Boroson, D. et al., "The Lunar Laser Communications Demonstration (LLCD)." In Third IEEE International Conference on Space Mission Challenges for Information Technology, SMC-IT 2009, pages 23–28. IEEE, 2009.

[7] Khatri, F. et al., "Lunar Laser Communication Demonstration operations architecture." Acta Astronautica 111 (2015) 77–83.

[8] Fields, R. et al. "NFIRE-to-TerraSAR-X laser communication results: satellite pointing, disturbances, and other attributes consistent with successful performance," Proc. SPIE 7330, Sensors and Systems for Space Applications III, 73300Q (6 May 2009); doi: 10.1117/12.820393.

[9] Long, M. J., "Pointing Acquisition and Tracking Design and Analysis for CubeSat Laser Communication Crosslinks," M.S. Thesis, Massachusetts Institute of Technology, February, 2018. http://hdl.handle.net/1721.1/115686

[10] Yoon, H., "Pointing System Performance Analysis for Optical Inter-satellite Communication on CubeSats," Ph.D Thesis, Massachusetts Institute of Technology, 2017. http://hdl.handle.net/1721.1/113743

[11] Raspberrypi.org, "BCM2837," [Online]. Available: https://www.raspberrypi.org/ documentation/hardware/raspberrypi/bcm2837/README.md. [Accessed 6/9/2018].

[12] Milanović, V., A. Kasturi, J. Yang, and F. Hu, "Closed-loop control of gimbal-less MEMS mirrors for increased bandwidth in LiDAR applications," SPIE Conference on Laser Radar Technology and Applications XXII, Anaheim, CA Apr. 12th, 2017. https://doi.org/10.1117/12.2264069

[13] Milanović, V. "Linearized Gimbal-less Two-Axis MEMS Mirrors," Optical Fiber Communication Conference and Exposition, San Diego, CA, Mar. 25, 2009. https://doi.org/10.1364/NFOEC.2009.JThA19

[14] Mirrorcletech.com, "Support," [Online]. Available: http://www.mirrorcletech.com/ support.php?order=3. [Accessed 6/9/2018]

[15] Cierny, O., "Precision Closed-Loop Laser Pointing System for the Nanosatellite Optical Downlink Experiment", M.S. Thesis, Luleå University of Technology and Julius Maximilians University of Würzburg, 2017.

[16] Guelman M., A. Kogan, A. Kazarian, A. Livne, M. Orenstein, M., H. Michalik, and S. Arnon, "Acquisition and pointing control for inter-satellite laser communications," IEEE Transactions on Aerospace and Electronic Systems, 40(4), 1239–1248, 2004. https://doi.org/10.1109/TAES.2004.1386877.

[17] Kaymak, Y., R. Rojas-Cessa, J. Feng, N. Ansari, M. Zhou, and T. Zhang, "A Survey on Acquisition, Tracking, and Pointing Mechanisms for Mobile Free-Space Optical Communications," IEEE Communications Surveys and Tutorials, 20(2), 1104–1123, 2018. https://doi.org/10.1109/COMST.2018.2804323.

[18] Hemmati, H., "Near-Earth Laser Communications," (H. Hemmati, Ed.), CRC Press, 2009. https://doi.org/10.1201/9781420015447

[19] Shields, J., and C. Pong, K. Lo, L. Jones, S. Mohan, C. Marom, L. Andrade, "Characterization of CubeSat Reaction Wheel Assemblies," Journal of Small Satellites, 6(1), 565–580, 2017.